The Cryosphere
Open Access
Discussions

Updated cloud physics improve the modelled near surface climate of Antarctica of a regional atmospheric climate model

J. M. van Wessem[1], C. H. Reijmer[1], J. T. M. Lenaerts[1], W. J. van de Berg[1], M. R. van den Broeke[1], and E. van Meijgaard[2]

[1]Institute for Marine and Atmospheric Research Utrecht, Utrecht University, Utrecht, the Netherlands
[2]Royal Netherlands Meteorological Institute, De Bilt, the Netherlands

Correspondence to: J. M. van Wessem (j.m.vanwessem@uu.nl)

Discussion Paper | Discussion Paper | Discussion Paper | Discussion Paper

TCD

7, 3231–3260, 2013

Effects of changed cloud physics

J. M. van Wessem et al.

Title Page

Abstract	Introduction
Conclusions	References
Tables	Figures

◄◄ | ►►

◄ | ►

Back | Close

Full Screen / Esc

Printer-friendly Version

Interactive Discussion

Abstract

The physics package of the polar version of the regional atmospheric climate model RACMO2 has been updated from RACMO2.1 to RACMO2.3. The update constitutes, amongst others, the inclusion of a parameterization for cloud ice super-saturation, an improved turbulent and radiative flux scheme and a changed cloud scheme. In this study the effects of these changes on the modelled near-surface climate of Antarctica are presented. Significant biases remain, but overall RACMO2.3 better represents the near-surface climate in terms of the modelled surface energy balance, based on a comparison with > 750 months of data from nine automatic weather stations located in East Antarctica. Especially the representation of the sensible heat flux and net longwave radiative flux has improved with a decrease in biases of up to 40 %. These improvements are mainly caused by the inclusion of ice super-saturation, which has led to more moisture being transported onto the continent, resulting in more and optically thicker clouds and more downward longwave radiation. As a result, modelled surface temperatures have increased and the bias, when compared to 10 m snow temperatures from 64 ice core observations, has decreased from −2.3 K to −1.3 K. The weaker surface temperature inversion consequently improves the representation of the sensible heat flux, whereas wind speed remains unchanged.

1 Introduction

Regional atmospheric climate models (RCMs) are important tools to improve our understanding of atmospheric processes and their relation to climate change as they provide amongst others the means to study the climate of areas where few observational data are available. RCMs have been successfully applied to remote areas such as Antarctica (e.g. van Lipzig et al., 2002) to assess the climate of the ice sheet (e.g. Van de Berg et al., 2005; Lenaerts et al., 2012b). Moreover, the RCMs are used to support remote sensing techniques such as GRACE (Chen et al., 2006), InSAR (Rig-

not et al., 2008), and provide a correction for firn densification in support of radar/laser altimetry (Ligtenberg et al., 2012). All techniques combined have recently provided reconciled mass balance estimates for the Greenland and Antarctic ice sheets (Shepherd et al., 2012).

The Regional Atmospheric Climate Model RACMO2, that has been adapted for specific use over the polar regions, has recently undergone a major update of its physics package. In the present study we show whether this update from version RACMO2.1 to RACMO2.3 has improved the representation of the Antarctic climate, with its extreme temperatures and winds. To do so we will assess the changes for Antarctica in the modelled surface energy balance (SEB), near-surface wind speeds and surface temperatures and compare these to available observations.

Section 2 discusses the model, the changes in model formulation and the observational data used for evaluation. In Sect. 3 the effects of the model changes on the SEB and the near-surface tem perature and wind are presented and a comparison is made to observational data, followed by a discussion in Sect. 4 and conclusions in Sect. 5.

2 Data and methods

2.1 RACMO2

RACMO2 combines the dynamical processes of the High Resolution Limited Area Model (HIRLAM) (Unden et al., 2002) with the physics package of the European Centre for Medium-range Weather Forecasts (ECMWF) Integrated Forecast System (IFS). RACMO2 has been specifically adapted for use over the large ice sheets of Greenland and Antarctica (e.g. Reijmer et al., 2005). It is interactively coupled to a multilayer snow model that calculates melt, percolation, refreezing and runoff of meltwater (Ettema et al., 2010; Greuell and Konzelmann, 1994). Surface albedo is based on a prognostic scheme for snow grain size (Kuipers Munneke et al., 2011) and a drifting snow routine simulates the interactions of drifting snow with the surface and the lower atmosphere

Title Page

Abstract | Introduction

Conclusions | References

Tables | Figures

◀ | ▶

◀ | ▶

Back | Close

Full Screen / Esc

Printer-friendly Version

Interactive Discussion

(Lenaerts et al., 2012b). A horizontal resolution of 27 km and a vertical resolution of 40 levels is used in order to resolve the significant complexity of the Antarctic climate. The model is forced by ERA-Interim re-analysis data (January 1979–December 2011, Dee et al., 2011) at the ocean and lateral boundaries, while the domain interior is allowed

5 to evolve freely.

Here we analyse changes in the modelled Antarctic near-surface climate after the ECMWF IFS physics package cycle CY23r4 in RACMO2.1 (White, 2001) has been updated to cycle CY33r1 in RACMO2.3 (ECWMF-IFS, 2008). The updates that have the most impact on Antarctic applications are the changes in the cloud scheme, the cloud

10 microphysics and the radiation and turbulence schemes. All changes will be described below and are discussed in more detail in relation with the results in Sect. 4.

An important change in the cloud scheme is the inclusion of a parameterization for ice super-saturation as described by Tompkins and Gierens (2007). As a result, the specific humidity of cold air parcels (at temperatures where the difference between liq-

15 uid water and ice saturation pressure is large) has to reach a higher value in order for condensation to occur. This leads to an improved representation of clouds and moisture concentrations in the (upper) troposphere (Tompkins and Gierens, 2007). Aircraft observations with the Microwave Limb Sounder (MLS) have shown that super-saturation frequently occurs over the steep coastal regions of Antarctica (Spichtinger et al., 2003).

20 Simulations with the ECMWF IFS have already shown that the new parameterization leads to a good global distribution of super-saturated atmospheres, albeit that a slight underestimation for Antarctica is still present (Tompkins and Gierens, 2007).

In the cloud microphysics scheme some parameterizations related to the formation of precipitation have been altered. This includes an increase of the auto-conversion

25 coefficient for convective clouds which determines the speed with which cloud content is converted into precipitation. The change leads to a more efficient and quicker formation of precipitation. It has been altered because updraft condensate was being overestimated in previous ECMWF model runs (ECWMF-IFS, 2008).

Effects of changed cloud physics

J. M. van Wessem et al.

Title Page

Abstract	Introduction
Conclusions	References
Tables	Figures

|◀ | ▶|

◀ | ▶

Back | Close

Full Screen / Esc

Printer-friendly Version

Interactive Discussion

Another change in the physics is the introduction of the McRad radiation scheme (Morcrette et al., 2008). It describes short- and longwave radiation transfer through clouds, based on the Monte Carlo Independent Column Approximation (McICA, Barker et al., 2008), and a revision of cloud optical properties making the parameterizations that use these properties more accurate. This improves the interaction of multi-layer cloud cover with short- and longwave radiation, but is believed to be of minor importance for Antarctica, considering the low occurrence frequency of these cloud types in this region. In the shortwave radiation scheme (SRTM, Mlawer and Clough, 1997) the Fouqart-Bonnel scheme is replaced by a scheme that is based on the correlated k-method (Lacis, 1991). The latter is shown to lead to an overall improved accuracy in calculated fluxes and heating rates (ECWMF-IFS, 2008).

The last relevant physics change is the newly implemented Eddy-Diffusivity Mass Flux (EDMF, Siebesma et al., 2007) scheme for boundary-layer turbulence/shallow convection. This scheme distinguishes between large-scale (updraughts) and small-scale (turbulence) mixing processes in the surface and boundary layer by describing them with either mass fluxes or diffusion.

The surface flux relies on Monin-Obukhov similarity theory but takes into account form drag (Beljaars et al., 2004) that is dependent on subscale orography. Especially for topographically rough areas like the Antarctic Peninsula these changes are expected to be important.

There are other minor changes in the model but these are of little significance in the context of this study. For instance the RACMO2 model update also incorporates changes in the HIRLAM dynamical core. These are mostly of numerical nature and are not adressed here. For a more detailed and complete description of the entire RACMO2 update the reader is referred to Van Meijgaard et al. (2012) and ECWMF-IFS (2008) and references therein.

2.2 Observational data

The near-surface wind, temperature and SEB are evaluated using observational data from nine automatic weather stations (AWS). Figure 1 shows the locations of the AWSs. They are located in different climate regimes: from relatively mild and wet coastal sites (AWS 4 and 11) to the steep escarpment region of Dronning Maud Land (DML) (AWS 5, 6 and 16), the South Dome of Berkner Island (AWS 10) and the high and cold East Antarctic plateau (AWS 8, 9 and 12). The datasets differ in quality, due to instrumental problems at some sites. Observation lengths range from 4 to 15 yr of data. A summary of the location and data records of the AWSs is provided in Table 1. All AWSs are of similar design: single level measurements of wind speed/direction, temperature and relative humidity are performed at a height of approximately 3 m. The individual radiation components (SW↓, SW↑, LW↓, LW↑) are measured with a single sensor. For more details see Van den Broeke et al. (2005a,b) and Reijmer and Oerlemans (2002).

The SEB can be written as:

$$M = \mathrm{SW_{net}} + \mathrm{LW_{net}} + \mathrm{SHF} + \mathrm{LHF} + G, \tag{1}$$

where fluxes directed towards the surface are defined positive with units $\mathrm{W\,m^{-2}}$, M is melt energy ($M = 0$ if the surface temperature $T_s < 273.15\,\mathrm{K}$), $\mathrm{SW_{net}}$ and $\mathrm{LW_{net}}$ are the net shortwave and longwave radiative fluxes, SHF and LHF are the sensible and latent heat fluxes and G is the subsurface conductive heat flux. The sensible- and latent heat fluxes are calculated using Monin-Obukhov similarity theory using the bulk method: see Van den Broeke et al. (2005b). Treatment of the radiation fluxes is as in Van den Broeke (2004). All data from the nine AWSs are monthly averaged and compared with data from the same months of the two RACMO cycles. An assessment of the quality of the observational data can be found in Reijmer and Oerlemans (2002); Van den Broeke et al. (2004). Note that the turbulent fluxes and surface temperatures are calculated values and not direct measurements.

As the AWSs only cover a part of East Antarctica, 64 ice core observations (Fig. 1) are additionally used to evaluate the spatial performance of RACMO2 for T_s. The mod-

elled surface temperature, averaged over 1979 to 2011, is compared to snow temperature measurements at 10 m depth similar to Van de Berg et al. (2007). The 10 m snow temperature is assumed to be representative for the annual mean surface temperature. Note that at 27 km, the observational data are compared with data from the nearest model grid point. For the 10 m snow temperatures, this causes four locations to fall outside of the ice mask. For these points the nearest grid point that does fall within the ice mask is used.

3 Results

3.1 General climate characteristics

In Antarctica a negative to zero radiation budget dominates the SEB year round. In winter, the radiation budget has to be balanced mainly by SHF, as LHF is generally small due to the low temperatures and thus small near-surface moisture gradients exist over the AIS. In summer the radiation budget regularly becomes positive due to absorption of shortwave radiation at the surface. The negative radiation budget prevails and cools the surface, resulting in a quasi-permanent surface-based temperature inversion. In combination with a sloping surface, this leads to the characteristic persistent katabatic winds over the AIS. As the cooling is stronger in winter, the katabatic winds increase in strength in winter. Stronger katabatic winds enhance downward sensible heat transport, which counteracts the strength of the surface temperature inversion by increasing the surface temperature. This results in a weaker seasonality of (near) surface temperature in high wind speed areas.

To illustrate this chain of events, Fig. 2 shows the monthly mean values of 10 m wind speed ($V_{10\,m}$), surface temperature (T_s), net longwave radiation (LW_{net}) and sensible heat flux (SHF) for four AWSs in different climate zones of the AIS (4, 5, 6 and 9). Figure 2a shows that monthly mean wind speeds for AWS 5 and 6, in the steep escarpment region, exhibit a strong seasonal cycle due to stronger katabatic forcing in winter, with

monthly wind speeds up to $9\,\mathrm{m\,s^{-1}}$. These katabatic winds mix warm air downward to the surface (large SHF), increasing surface temperature (Fig. 2b), and hence longwave cooling (Fig. 2c). For AWS 4 and AWS 9, located on the relatively flat coastal ice shelf and interior ice sheet, respectively, wind speeds are lower, non-katabatic and show no

5 seasonal cycle. At these sites the seasonal amplitude in temperature is larger than at the sites dominated by katabatic winds (AWS 5 and 6) mainly because the wintertime surface inversion is stronger.

3.2 Simulation of wind speed and temperature

Figure 3 shows the correlation (r) (Fig. 3a, c) and difference (model–observation)

10 (Fig. 3b, d) of the monthly averaged wind speed and surface temperature of all nine AWSs (>750 months) as a function of the observed value for RACMO2.3 and RACMO2.1. Figure 3a, b shows that RACMO2.3 does not improve the wind speed representation when compared to RACMO2.1 (for both datasets: bias = 0.5, $r = 0.53$ with significance level $p < 0.0001$), of which the representation was already good (Lenaerts

15 et al., 2012b). Both model cycles generally underestimate high wind speeds and overestimate low wind speeds. Since near-surface winds over the AIS are dominated by katabatic forcing, this is caused by an overestimation of surface slopes in flat areas (AWS 4, 8, 9, 10, 12) and an underestimation of surface slopes in steep areas (AWS 5, 6, 11) owing to the steep terrain of the escarpment region in DML, in combination with

20 the limited horizontal resolution of the model (Reijmer et al., 2005). To investigate the seasonal effects, Fig. 4a shows the monthly mean difference (model – observation) of $V_{10\,\mathrm{m}}$ for AWS 4, 5, 6 and 9 respectively. For AWS 5 and AWS 6 (slope $> 10\,\mathrm{m\,km^{-1}}$) wind speed is underestimated year round. For AWS 4 and AWS 9 the wind speed is overestimated in winter when katabatic forcing is overestimated and therefore shows

25 a seasonality that is too pronounced. This has a strong effect on the temperature as shown in Fig. 4b,c where temperature is underestimated at AWS 5 and 6. The surface temperature inversion, defined here as $T_{\mathrm{inv}} = T_{2\,\mathrm{m}} - T_{\mathrm{s}}$, is underestimated when wind

speed is overestimated (Fig. 4d) implying that the bias in T_s is more positive than the bias in T_{2m}.

In contrast to wind speed, a clear improvement in surface temperature T_s (Fig. 3c, d) in RACMO2.3 over RACMO2.1 is seen, where the cold bias has been reduced from 3.3 K to 1.9 K while the correlation has hardly changed ($r = 0.95$ in RACMO2.1 and $r = 0.96$ in RACMO2.3, $p < 0.0001$). This improvement occurs year-round for the AWSs except for AWS 4, where the representation was already good due to the overestimated wind speed. A comparison of monthly averaged V_{10m} and T_{2m} from the Reference Antarctic Data for Environmental Research (READER, Turner et al., 2005) AWS and surface station data showed similar results. In order to adress the improvement in the T_s representation, we discuss the SEB in the next section.

3.3 Surface energy balance

Figure 5 shows the difference of the monthly averaged modeled and observed SEB fluxes for all AWS. The average bias and correlation coefficients are summarized in Table 2. Most biases are reduced in RACMO2.3: for SHF from $10.6\,\mathrm{W\,m^{-2}}$ to $7.1\,\mathrm{W\,m^{-2}}$, for LW_{net} from $-10.3\,\mathrm{W\,m^{-2}}$ to $-6.3\,\mathrm{W\,m^{-2}}$. The changes in LHF and SW_{net} are small. For SW_{net} the bias increased from $-1.6\,\mathrm{W\,m^{-2}}$ to $-2.0\,\mathrm{W\,m^{-2}}$ but the representation was already good ($r = 0.97$). For LHF the slight improvement from $0.6\,\mathrm{W\,m^{-2}}$ to $0.4\,\mathrm{W\,m^{-2}}$ is of little significance due to its small magnitude and the uncertainty of the observed fluxes.

The most important improvement is that of LW_{net}, although it remains too negative, due to a too small LW↓ (Van de Berg et al., 2007). Figure 6 shows the monthly mean difference of SEB fluxes for AWS 4, 5, 6 and 9, and shows that LW_{net} is underestimated at all AWS locations, and most significantly at AWS 4 and 9. The overestimated slope at these two sites triggers a katabatic feedback in winter, resulting in overestimated SHF. In RACMO2.3, the improved LW↓ reduces this problem.

The underestimated slope results in too low wind speeds at AWS 5 and 6, resulting in an overestimation of the surface temperature inversion (Fig. 4d). As a result, SHF is reasonably well represented, because stability effects remain small even at the underestimated wind speeds (Van den Broeke et al., 2005b). The problem is further reduced in RACMO2.3, in which the SEB at AWS 5 and 6 is well represented.

In summer the SHF bias at AWS 4 is smaller because SW_{net} and LHF help to balance the excess longwave cooling. For AWS 9 however, there is an increased negative bias in SW_{net} in RACMO2.3 due to an overestimated albedo. In general, for all sites the improved representation of SEB components are mostly induced by a better representation of LW↓, but also changes in the turbulence scheme (section 4) contribute to the improvement.

Figure 5a confirms that high wintertime SHF values in the escarpment zone are well represented, and that RACMO2 generally overestimates SHF in flatter areas. This leads to overestimated T_s and hence too negative LW_{net} (Fig. 5d). Both biases are significantly reduced in RACMO2.3, by 33 % (SHF) and 39 % (LW_{net}) respectively. In summer, RACMO2 underestimates SW_{net} in the high interior (Fig. 5c). As a result, T_s is underestimated (Figs. 3c, d and 4c), the surface temperature inversion overestimated as well as SHF (Figs. 5a, 6d). As a result of too low T_s, sublimation (negative LHF) is underestimated and summertime convection (upward SHF) does not take place on the ice sheet.

3.4 Spatial variations in T_s

Since the AWS are located mainly in DML, which has a topography that is not typical for the entire ice sheet, we use 10 m snow temperature data to obtain a better spatial coverage of the T_s evaluation (Fig. 1). Figure 7 shows the difference between modeled and observed T_s as a function of the latter, averaged over the model timespan. Average values, bias and correlation are given in Table 2. Surface temperatures in RACMO2.1 are underestimated at almost all locations and on average are too low by 2.3 K. RACMO2.3 reduces this bias to −1.3 K. Overall the spatial variability of surface

Title Page

Abstract	Introduction
Conclusions	References
Tables	Figures

|◄ | ►|

◄ | ►

Back | Close

Full Screen / Esc

Printer-friendly Version

Interactive Discussion

temperatures is well represented by both model versions ($r = 0.98$ for RACMO2.1 and $r = 0.99$ for RACMO2.3, $p < 0.0001$) although there seems to be a tendency towards larger underestimations at higher temperature locations.

To further illustrate this, Fig. 8 shows the spatial pattern of (a) T_s and (b) surface potential temperature θ_s for RACMO2.3 including the observations. The best agreement is found on the cold East Antarctic plateau, where the overestimated wind speeds compensate the bias in temperature caused by the underestimated LW↓. Because of the improved LW↓, T_s has changed from being slightly underestimated in RACMO2.1 to being slightly overestimated in RACMO2.3. In West Antarctica and the coastal margins, T_s is underestimated the most, due to both $V_{10\,m}$ and LW$_{net}$ being underestimated and here RACMO2.3 produces the largest improvement. Figure 8b shows the potential temperature, compensating for elevation differences and showing the katabatic wind zone where potential temperatures are high and the model matches the observations well.

These changes are also seen in Fig. 9 where the difference fields (RACMO2.3 – RACMO2.1) for LW$_{net}$, T_s, $V_{10\,m}$ and SHF are shown. The decrease in longwave cooling LW$_{net}$ (Fig. 9a) is found for most of the AIS and is strongest on the East Antarctic plateau. This results in higher T_s (Fig. 9b) and leads to a decrease in SHF (Fig. 9d) similar to the decrease in LW$_{net}$ but less strong due to the added effects of SW$_{net}$ and LHF in summer. A related pattern in wind speed is not seen (Fig. 9c), with changes in $V_{10\,m}$ smaller than 5%. Differences in $V_{10\,m}$ are due to the combined effect of model changes but the errors in wind speed with respect to the observations are dominated by the model topography (note that the model topography is the same in both model cycles).

4   Discussion

The updated physics cycle in RACMO2 results in significant changes in the modelled near-surface climate of the AIS, particularly LW↓; the new parameterization for ice

super-saturation changes the total amount of modelled clouds over Antarctica, most notably over the East Antarctic plateau. To illustrate this effect, Fig. 10 shows a latitudinal cross-section of the vertical distribution of total cloud water/ice content, averaged over the period 2007–2010 (representative for the entire simulation). A significant increase of modelled cloud content is found over the East Antarctic plateau, while cloud content has decreased along the coastline and over the ocean. With the new parameterization, moist air that reaches the continent has to exceed 100% relative humidity up to 150% in order to form clouds. As a result, clouds form further inland and higher up in the troposphere, resulting in more clouds simulated by RACMO2.3 in the interior.

The increase in clouds is consistent with the decreased bias in LW_{net} presented in Sect. 3. The underestimation of $LW{\downarrow}$ was the main cause of the bias in LW_{net} (Van de Berg et al., 2007), and the bias is now reduced. These improvements have led to higher surface temperatures, reducing the temperature gradients in the surface layer and resulting in lower SHF values, mainly in winter. The bias in SW_{net} is the only bias that has increased, albeit slightly. This is caused by a general overestimation of surface albedo at plateau stations AWS 9 and 12 (Van de Berg et al., 2007) that has increased in RACMO2.3 due to more fresh snowfall. For AWSs located closer to the coast the bias remained the same and is generally small.

To assess the impact of changes in the atmospheric surface layer scheme Figure 11 shows monthly averaged SHF for all AWSs, RACMO2.3 and RACMO2.1 as a function of the surface temperature inversion and wind speed (color scheme). The filled circles represent winter conditions (April–September), open circles conditions for October–March. Figure 11a clearly shows three regimes. Regime II represents the katabatic wind zone where SHF increases quadratically with the katabatic wind forcing (inversion strength). Regime III represents the stable conditions of the AWSs in flat areas where static stability effects become important at high values of the temperature inversion, suppressing SHF. Regime IV represents the exceptional conditions at AWS 16, where despite stable conditions and low wind speeds, SHF values are high due to large scale circulation effects. The model (Fig. 11b,c) does not simulate this regime accurately due

to the limited spatial resolution as the station is positioned in a topographically complex region.

For lower stabilities and towards summer conditions the branches join and SHF shows a linear dependence on T_{inv}, indicating the convective summertime conditions at plateau stations AWS 9 and 12 (Regime I). This regime is exclusively found on the plateau, where the low summertime temperatures prevent sublimation (LHF) to act as a surface energy sink. Because RACMO2 overestimates albedo and underestimates atmospheric transmissivity, a positive radiation balance is not simulated (at least not in the monthly mean sense).

Figure 11b, c shows the inability of RACMO2 to simulate regimes I and IV. The behaviour in the katabatic wind zone is represented well, although the branch is less pronounced due to the underestimation of the slope and hence wind speeds. RACMO2.3 simulates an improved separation of the most important regimes II and III compared to RACMO2.1, because of the improved surface layer turbulence scheme and general changes in the simulated results.

5 Conclusions

The ECMWF physics package of the regional atmospheric climate model RACMO2 has been upgraded from cycle CY23r4 (RACMO2.1) to CY33r1 (RACMO2.3). This study evaluates the effects of this change on the surface energy balance (SEB), 10 m wind speed $V_{10\,m}$ and surface temperature T_s by comparing both cycles with observational SEB data gathered from 9 automatic weather stations in East Antarctica and 64 deep snow temperature sites. The model has improved in several aspects. In RACMO2.3 the biases in the sensible heat flux (SHF) and the net longwave radiation (LW$_{net}$) have decreased from 10.3 to 6.3 W m^{-2} and −10.6 to −7.1 W m^{-2}, respectively. This is mainly caused by more clouds in the interior and increased cloud optical thickness resulting in more downward longwave radiation. Inclusion of a parameterization for ice supersaturation has led to increased moisture content in the atmosphere and more clouds

in the upper troposphere. The change in longwave radiation has improved the bias in the SHF through its tight coupling with T_s and wind speed: the bias in T_s has decreased from $-2.4\,\mathrm{K}$ to $-1.3\,\mathrm{K}$. 2 Meter temperatures have also increased but in a smaller magnitude than T_s, decreasing the surface-based temperature inversion. The bias in $V_{10\,\mathrm{m}}$ is mainly due to the flattened ice sheet topography, and remains unchanged.

References

Barker, H. W., Cole, J. N. S., Morcrette, J., and Pincus, R.: The Monte Carlo independent column approximation: an assessment using several global atmospheric models, Q. J. Roy. Meteorol. Soc., 1478, 1463–1478, doi:10.1002/qj.303, 2008. 3235

Beljaars, A. C., Brown, A. R., and Wood, N.: A new parametrization of turbulent orographic form drag, Q. J. Roy. Meteorol. Soc., 130, 1327–1347, doi:10.1256/qj.03.73, 2004. 3235

Chen, J. L., Wilson, C. R., Blankenship, D. D., and Tapley, B. D.: Antarctic mass rates from GRACE, Geophys. Res. Lett., 33, L11502, doi:10.1029/2006GL026369, 2006. 3232

Dee, D. P., Uppala, S. M., Simmons, A. J., Berrisford, P., Poli, P., Kobayashi, S., Andrae, U., Balmaseda, M. A., Balsamo, G., Bauer, P., Bechtold, P., Beljaars, A. C. M., Van de Berg, L., Bidlot, J., Bormann, N., Delsol, C., Dragani, R., Fuentes, M., Geer, A. J., Haimberger, L., Healy, S. B., Hersbach, H., Hólm, E. V., Isaksen, L., Kå llberg, P., Köhler, M., Matricardi, M., McNally, A. P., Monge-Sanz, B. M., Morcrette, J. J., Park, B. K., Peubey, C., de Rosnay, P., Tavolato, C., Thépaut, J. N., and Vitart, F.: The ERA-Interim reanalysis: configuration and performance of the data assimilation system, Q. J. Roy. Meteorol. Soc., 137, 553–597, doi:10.1002/qj.828, 2011. 3234

ECMWF-IFS: Part IV : Physical Processes (CY33R1), Tech. Rep. June, available at: http://www.ecmwf.int/research/ifsdocs/CY33r1/PHYSICS/IFSPart4.pdf, 2008. 3234, 3235

Ettema, J., van den Broeke, M. R., van Meijgaard, E., van de Berg, W. J., Box, J. E., and Steffen, K.: Climate of the Greenland ice sheet using a high-resolution climate model – Part 1: Evaluation, The Cryosphere, 4, 511–527, doi:10.5194/tc-4-511-2010, 2010. 3233

Greuell, W. and Konzelmann, T.: Numerical modelling of the energy balance and the englacial temperature of the Greenland Ice Sheet. Calculations for the ETH-Camp location (West Greenland, 1155 m a.s.l.), Global Planet. Change, 9, 91–114, doi:10.1016/0921-8181(94)90010-8, 1994. 3233

Kuipers Munneke, P., Van den Broeke, M. R., Lenaerts, J. T. M., Flanner, M. G., Gardner, A. S., and Van de Berg, W. J.: A new albedo parameterization for use in climate models over the Antarctic ice sheet, J. Geophys. Res., 116, 1–10, doi:10.1029/2010JD015113, 2011. 3233

Lacis, A.: A description of the correlated k distribution method for modeling nongray gaseous absorption, thermal emission, and multiple scattering in vertically inhomogeneous atmospheres to N_2. Comparison cooling, J. Geophys. Res., 96, 9027–9063, 1991. 3235

Lenaerts, J. T. M., van den Broeke, M. R., Déry, S. J., van Meijgaard, E., van de Berg, W. J., Palm, S. P., and Sanz Rodrigo, J.: Modeling drifting snow in Antarctica with a regional climate model: 1. Methods and model evaluation, J. Geophys. Res., 117, 1–17, doi:10.1029/2011JD016145, 2012a.

Lenaerts, J. T. M., Van den Broeke, M. R., Van de Berg, W. J., Mei, E. V., and Kuipers Munneke, P.: A new high-resolution surface mass balance map of Antarctica (1979–2010) based on regional atmospheric climate modeling, Geophys. Res. Lett., 39, 1–5, doi:10.1029/2011GL050713, 2012b. 3232, 3234, 3238

Ligtenberg, S. R. M., Horwath, M., van den Broeke, M. R., and Legrésy, B.: Quantifying the seasonal "breathing" of the Antarctic ice sheet, Geophys. Res. Lett., 39, L23501, doi:10.1029/2012GL053628, 2012. 3233

Liu, H., Jezek, K., Li, B., and Zhao, Z.: Radarsat Antarctic Mapping Project digital elevation model version 2, Tech. rep., 2001. 3248, 3250

Mlawer, E. J. and Clough, S. A.: Shortwave and Longwave Enhancements in the Rapid Radiative Transfer Model, in: Proc. 7th Atmospheric Radiation Measurement (ARM) Science Team Meeting, 1992, 409–413, 1997. 3235

Morcrette, J.-J., Barker, H. W., Cole, J. N. S., Iacono, M. J., and Pincus, R.: Impact of a New Radiation Package, McRad, in the ECMWF Integrated Forecasting System, Mon. Weather Rev., 136, 4773–4798, doi:10.1175/2008MWR2363.1, 2008. 3235

Reijmer, C. H. and Oerlemans, J.: Temporal and spatial variability of the surface energy balance in Dronning Maud Land, East Antarctica, J. Geophys. Res., 107, doi:10.1029/2000JD000110, 2002. 3236

Effects of changed cloud physics

J. M. van Wessem et al.

Title Page

Abstract | Introduction

Conclusions | References

Tables | Figures

◄ | ►

Back | Close

Full Screen / Esc

Printer-friendly Version

Interactive Discussion

Reijmer, C. H., Van Meijgaard, E., and Van den Broeke, M. R.: Evaluation of temperature and wind over Antarctica in a Regional Atmospheric Climate Model using 1 year of automatic weather station data and upper air observations, J. Geophys. Res., 110, 1–12, doi:10.1029/2004JD005234, 2005. 3233, 3238

5 Rignot, E., Bamber, J. L., Van den Broeke, M. R., Davis, C., Li, Y., Van de Berg, W. J., and Van Meijgaard, E.: Recent Antarctic ice mass loss from radar interferometry and regional climate modelling, Nat. Geosci., 1, 106–110, doi:10.1038/ngeo102, 2008. 3232

Shepherd, A., Ivins, E. R., Geruo, A., Barletta, V. R., Bentley, M. J., Bettadpur, S., Briggs, K. H., Bromwich, D. H., Forsberg, R., Galin, N., Horwath, M., Jacobs, S., Joughin, I., King, M. A.,

10 Lenaerts, J. T. M., Li, J., Ligtenberg, S. R. M., Luckman, A., Luthcke, S. B., McMillan, M., Meister, R., Milne, G., Mouginot, J., Muir, A., Nicolas, J. P., Paden, J., Payne, A. J., Pritchard, H., Rignot, E., Rott, H., Sørensen, L. S., Scambos, T. A., Scheuchl, B., Schrama, E. J. O., Smith, B., Sundal, A. V., van Angelen, J. H., van de Berg, W. J., van den Broeke, M. R., Vaughan, D. G., Velicogna, I., Wahr, J., Whitehouse, P. L., Wingham, D. J., Yi, D., Young,

15 D., and Zwally, H. J.: A reconciled estimate of ice-sheet mass balance, Science, 338, 1183–1189, doi:10.1126/science.1228102, 2012. 3233

Siebesma, A. P., Soares, P. M. M., and Teixeira, J. A.: A combined eddy-diffusivity mass-flux approach for the convective boundary layer, J. Atmos. Sci., 64, 1230–1248, doi:10.1175/JAS3888.1, 2007. 3235

20 Spichtinger, P., Gierens, K., and Read, W.: The global distribution of ice-supersaturated regions as seen by the Microwave Limb Sounder, Q. J. Roy. Meteorol. Soc., 129, 3391–3410, doi:10.1256/qj.02.141, 2003. 3234

Tompkins, A. M. and Gierens, K.: Ice supersaturation in the ECMWF integrated forecast, Q. J. Roy. Meteorol. Soc., 133, 53–63, doi:10.1002/qj, 2007. 3234

25 Turner, J., Colwell, S. R., Marshall, G. J., Lachlan-Cope, T. A., Carleton, A. M., Jones, P. D., Lagun, V., Reid, P. A., and Iagovkina, S.: Antarctic climate change during the last 50 years, Int. J. Climatol., 25, 279–294, doi:10.1002/joc.1130, 2005. 3239

Unden, P., Rontu, L., Jarvinen, H., Lynch, P., Calvo, J., Cats, G., Cuxart, J., Eerola, K., Fortelius, C., Garcia-moya, J. A., Jones, C., Lenderlink, G., Mcdonald, A., Mcgrath, R., and Navascues,

30 B.: HIRLAM-5 Scientific Documentation, Tech. Rep. December, Swedish Meteorology and Hydrology Institute, 2002. 3233

Van de Berg, W. J., Van den Broeke, M. R., Reijmer, C. H., and Van Meijgaard, E.: Characteristics of the Antarctic surface mass balance, 1958–2002, using a regional atmospheric climate model, Ann. Glaciol., 41, 97–104, doi:10.3189/172756405781813302, 2005. 3232

Van de Berg, W. J., Van den Broeke, M. R., and van Meijgaard, E.: Heat budget of the East Antarctic lower atmosphere derived from a regional atmospheric climate model, J. Geophys. Res., 112, D23101, doi:10.1029/2007JD008613, 2007. 3237, 3239, 3242

Van den Broeke, M. R.: Surface radiation balance in Antarctica as measured with automatic weather stations, J. Geophys. Res., 109, 1–17, doi:10.1029/2003JD004394, 2004. 3236, 3251

Van den Broeke, M. R., Van As, D., Reijmer, C. H., and Van de Wal, R. S. W.: Assessing and improving the quality of unattended radiation observations in Antarctica, J. Atmos. Ocean. Technol., 21, 1417–1431, doi:10.1175/1520-0426(2004)021<1417:AAITQO>2.0.CO;2, 2004. 3236

Van den Broeke, M. R., Reijmer, C. H., and As, D. V.: Seasonal cycles of Antarctic surface energy balance from automatic weather stations, Ann. Glaciol., 41, 131–139, 2005a. 3236

Van den Broeke, M. R., Van As, D., Reijmer, C. H., and Van de Wal, R. S. W.: Sensible heat exchange at the Antarctic snow surface: a study with automatic weather stations, Int. J. Climatol., 25, 1081–1101, doi:10.1002/joc.1152, 2005b. 3236, 3240

van Lipzig, N. P. M., Meijgaard, E. V., and Oerlemans, J.: The spatial and temporal variability of the surface mass balance in Antarctica: results from a regional atmospheric climate model, Int. J. Climatol., 22, 1197–1217, doi:10.1002/joc.798, 2002. 3232

Van Meijgaard, E., Van Ulft, L., Lenderink, G., Roode, S. D., Wipfler, L., Boers, R., and Timmermans, R.: Refinement and application of a regional atmospheric model for climate scenario calculations of Western Europe, Tech. rep., 2012. 3235

White, P. W.: Part IV: PHYSICAL PROCESSES (CY23R4), Tech. Rep. September, 2001. 3234

Table 1. The AWS topographic characteristics and period of operation (until December 2011). Nr. months represents the number of available months over the model period (January 1979–December 2011). If no end time is indicated, the AWS is still operational end of 2011. Observed surface slope ($m\,km^{-1}$) is based on a $1\,km \times 1\,km$ Digital Elevation Model (Liu et al., 2001), modelled surface slope is based on the 27 km interpolated grid.

AWS	4	5	6	8	9	10	11	12	16
Latitude	72°45′ S	73°06′ S	74°28′ S	76°00′ S	75°00′ S	79°34′ S	71°09′ S	78°39′ S	71°57′ S
Longitude	15°29.9′ W	13°09.9′ W	11°31.0′ W	08°03′ W	00°00′ E/W	45°47′ W	06°42′ W	35°38′ E	23°20′ E
Elevation (obs)	34 m	363 m	1160 m	2400 m	2892 m	890 m	700 m	3620 m	1300 m
Elevation (mod)	23 m	332 m	1219 m	2405 m	2856 m	789 m	224 m	3621 m	1130 m
Slope (obs)	1.0	23.1	38.4	2.0	1.5	1.1	15.5	2.0	15.6
Slope (mod)	3.4	7.8	28.9	3.5	2.0	5.1	10.7	2.2	16.2
Start	Dec 1997	Feb 1998	Jan 1998	Jan 1998	Dec 1997	Jan 2001	Jan 2007	Dec 2007	Feb 2009
End	Dec 2002	–	Jan 2009	Jan 2003	–	Jan 2006	–	–	–
nr. months	60/60	167/167	134/134	19/44	162/168	48/54	57/59	49/49	29/35

Table 2. Mean, bias and correlation coefficient for sensible heat flux (SHF), latent heat flux (LHF), net shortwave radiation (SW$_{net}$), net longwave radiation (LW$_{net}$), 10 m wind speed ($V_{10\,m}$) and surface temperature T_s as modelled by RACMO2.1 and RACMO2.3 and as observed with the 9 AWS's (> 750 months). Also shown are the values for annual averaged T_s in comparison with 10 meter snow temperatures from 64 ice core measurements. For all data the significance level $p < 0.0001$.

		Obs mean	RACMO2.1 mean	bias	r	RACMO2.3 mean	bias	r
SHF	[W m^{-2}]	14.24	24.69	10.46	0.75	21.3	7.07	0.78
LHF	[W m^{-2}]	−2.11	−1.56	0.56	0.56	−1.75	0.37	0.62
SW$_{net}$	[W m^{-2}]	22.73	21.39	−1.34	0.97	20.76	−1.97	0.96
LW$_{net}$	[W m^{-2}]	−35.03	−45.38	−10.34	0.81	−41.33	−6.29	0.81
$V_{10\,m}$	[m s^{-1}]	6.38	5.9	−0.48	0.53	5.88	−0.51	0.53
T_s (AWS)	[K]	244.28	241.04	−3.24	0.95	242.41	−1.86	0.96
T_s (ice cores)	[K]	240.6	238.28	−2.32	0.98	239.3	−1.28	0.99
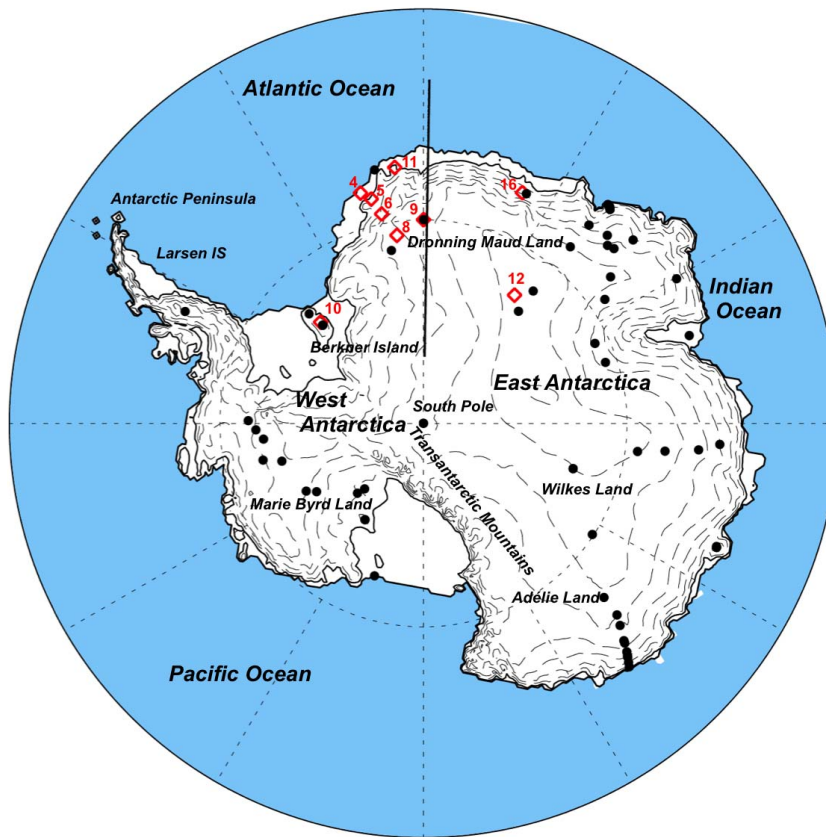
Fig. 1. Map of Antarctica with locations of the AWS (red diamonds) the 64 coring sites (black dots) and the position of the latitudinal cross-section used in Fig. 10. Also shown are the ice-shelf edge and grounding line (solid lines) and height intervals every 500 m (dashed lines) based on a digital elevation model from Liu et al. (2001).
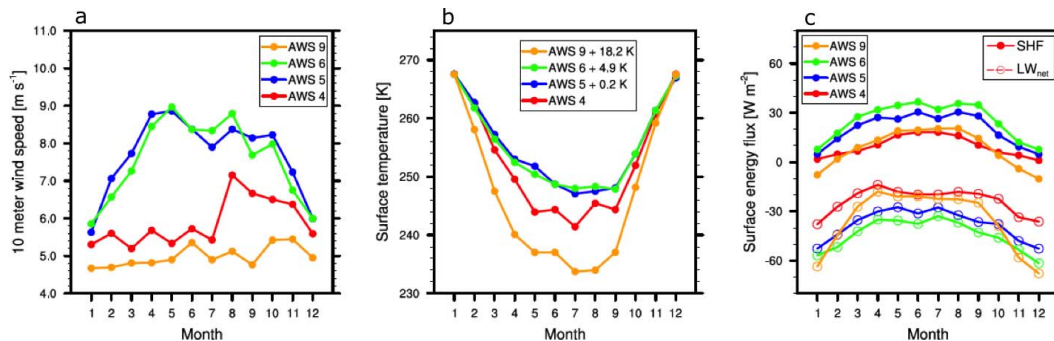
Fig. 2. Monthly mean **(a)** 10 m wind speed ($V_{10\,m}$), **(b)** surface temperature (T_s) and **(c)** sensible heat flux (SHF) and net longwave radiation (LW_{net}) for AWS 4, AWS 5, AWS 6 and AWS 9. The temperature curves for AWS 5, 6 and 9 (Fig. 2b) are shifted upward by 0.2, 4.9 and 18.2 K respectively, to correct for elevation and continentality differences (Van den Broeke, 2004).
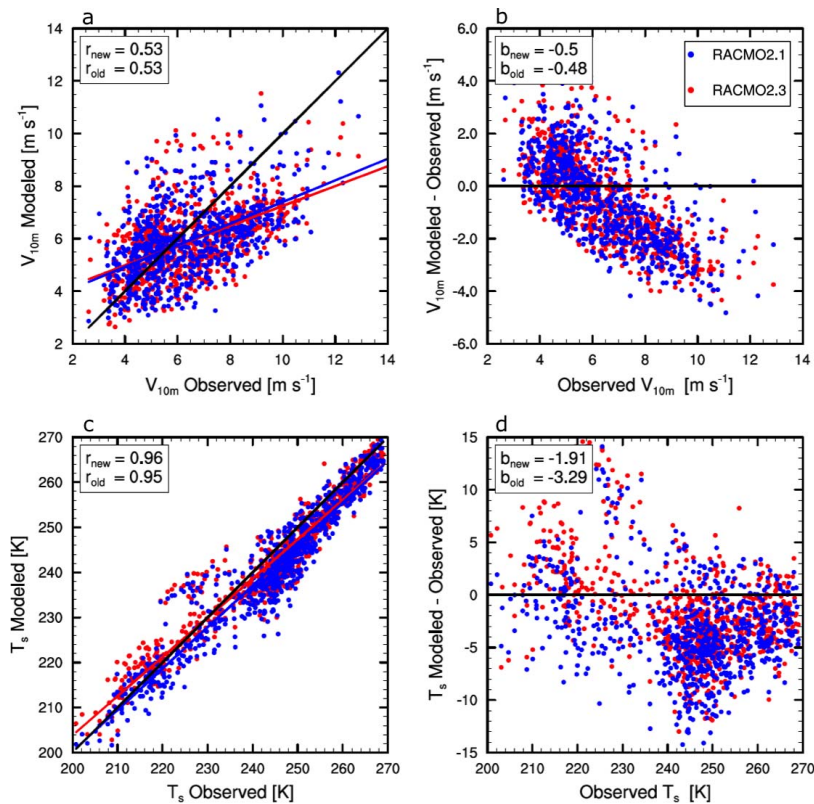
Fig. 3. Modelled and difference (modelled – observed) as a function of the AWS observations of **(a, b)** monthly averaged 10 m wind speed ($V_{10\,m}$) and **(c, d)** surface temperature (T_s). Shown are RACMO2.3 (red) with correlation r_{new} and bias b_{new} and RACMO2.1 (blue) with correlation r_{old} and bias b_{old}. Biases are averages over all data with units [m s^{-1}] for $V_{10\,m}$ and [K] for T_s.

Discussion Paper | Discussion Paper | Discussion Paper | Discussion Paper |

TCD

7, 3231–3260, 2013

Effects of changed cloud physics

J. M. van Wessem et al.

Title Page

Abstract | Introduction

Conclusions | References

Tables | Figures

|◀ | ▶|

◀ | ▶

Back | Close

Full Screen / Esc

Printer-friendly Version

Interactive Discussion
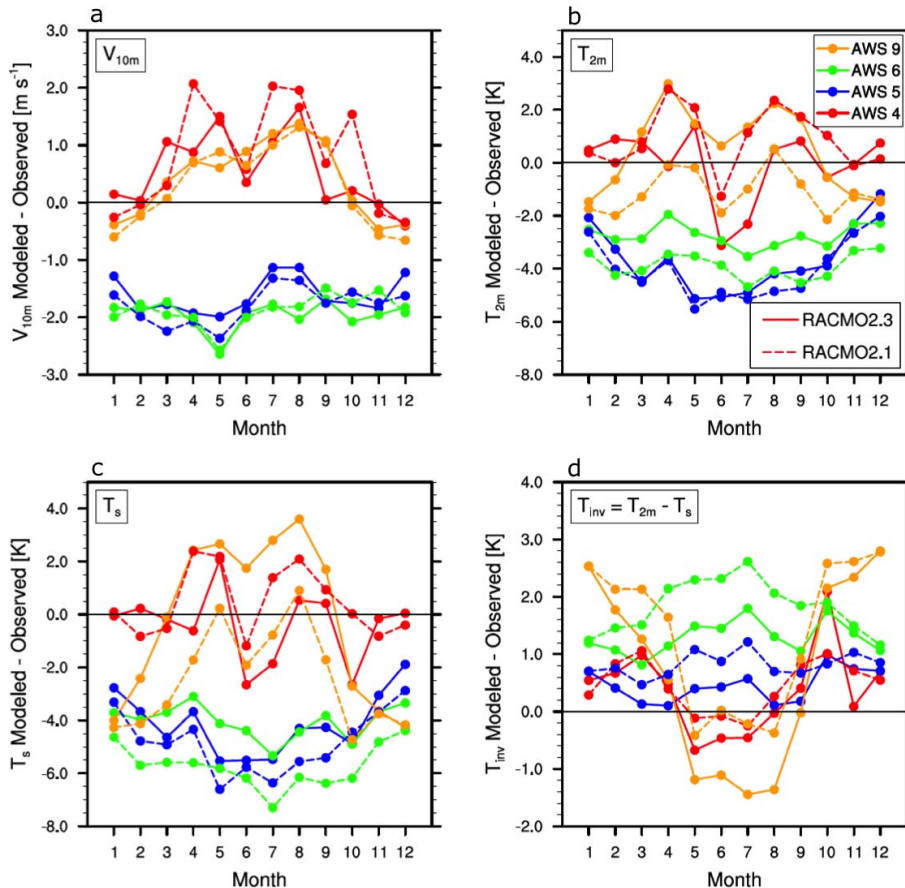
Fig. 4. Annual cycle of monthly mean difference (modelled – observed) of **(a)** 10 m wind speed (V_{10m}), **(b)** 2 m temperature (T_{2m}), **(c)** surface temperature (T_s) and **(d)** the surface temperature inversion ($T_{inv} = T_{2m} - T_s$) for AWS 4, AWS 5, AWS 6 and AWS 9. Shown are RACMO2.3 (solid line) and RACMO2.1 (dashed line).
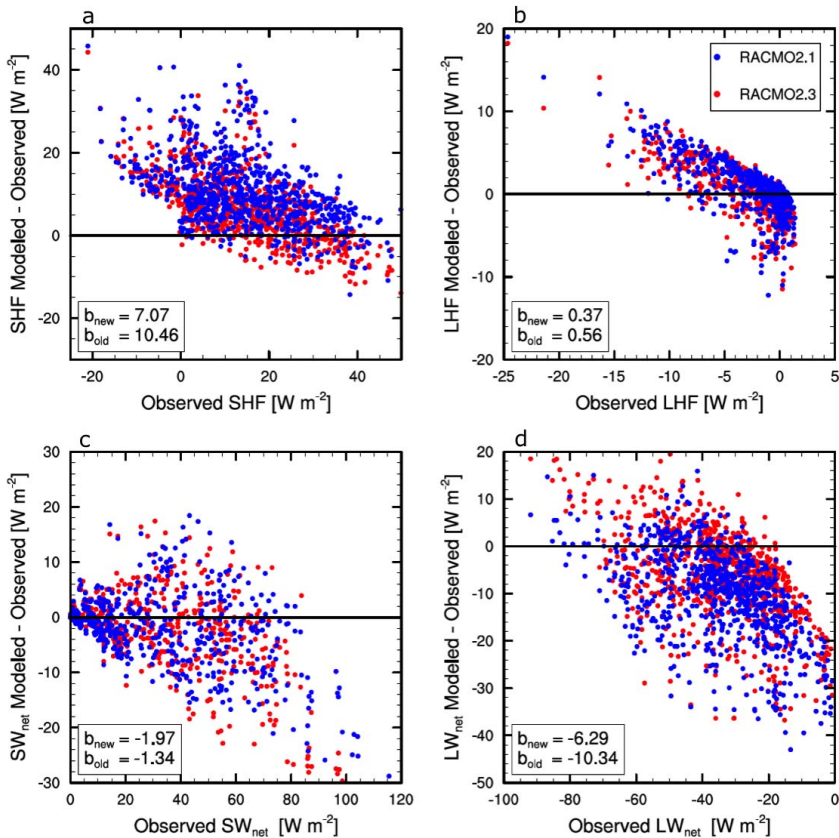
Fig. 5. Difference (modelled – observed) of **(a)** sensible heat flux (SHF), **(b)** latent heat flux (LHF), **(c)** net shortwave radiation (SW$_{net}$) and **(d)** net longwave radiation (LW$_{net}$) as a function of the AWS observations. Shown are RACMO2.3 (red) with bias b_{new} and RACMO2.1 (blue) with bias b_{old}. Biases (in [W m^{-2}]) are averages over all monthly average weather station data (> 750 data points).

Title Page

Abstract · Introduction

Conclusions · References

Tables · Figures

|◄ · ►|

◄ · ►

Back · Close

Full Screen / Esc

Printer-friendly Version

Interactive Discussion
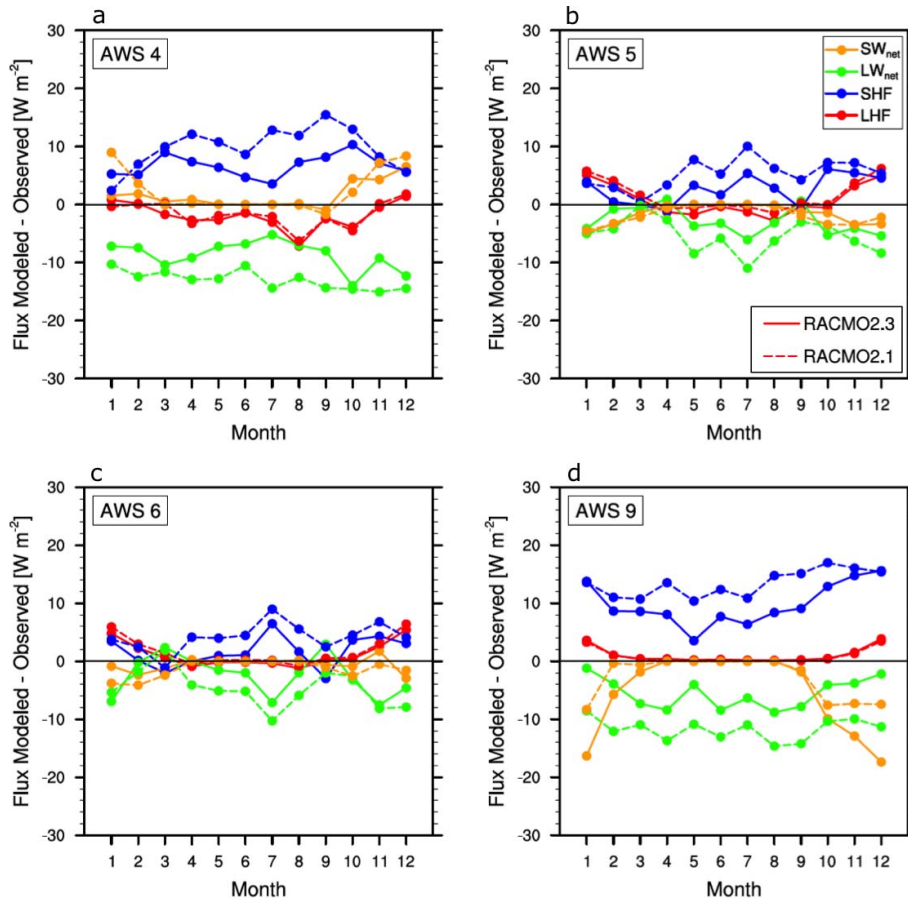
Fig. 6. Annual cycle of monthly mean difference (modelled – observed) of the SEB components (SHF (blue), LHF (red), SW$_{net}$ (orange), LW$_{net}$ (green)) for **(a)** AWS 4, **(b)** AWS 5, **(c)** AWS 6 and **(d)** AWS 9. Shown are RACMO2.3 (solid line) and RACMO2.1 (dashed line).

Title Page

Abstract | Introduction

Conclusions | References

Tables | Figures

|◀ | ▶|

◀ | ▶

Back | Close

Full Screen / Esc

Printer-friendly Version

Interactive Discussion
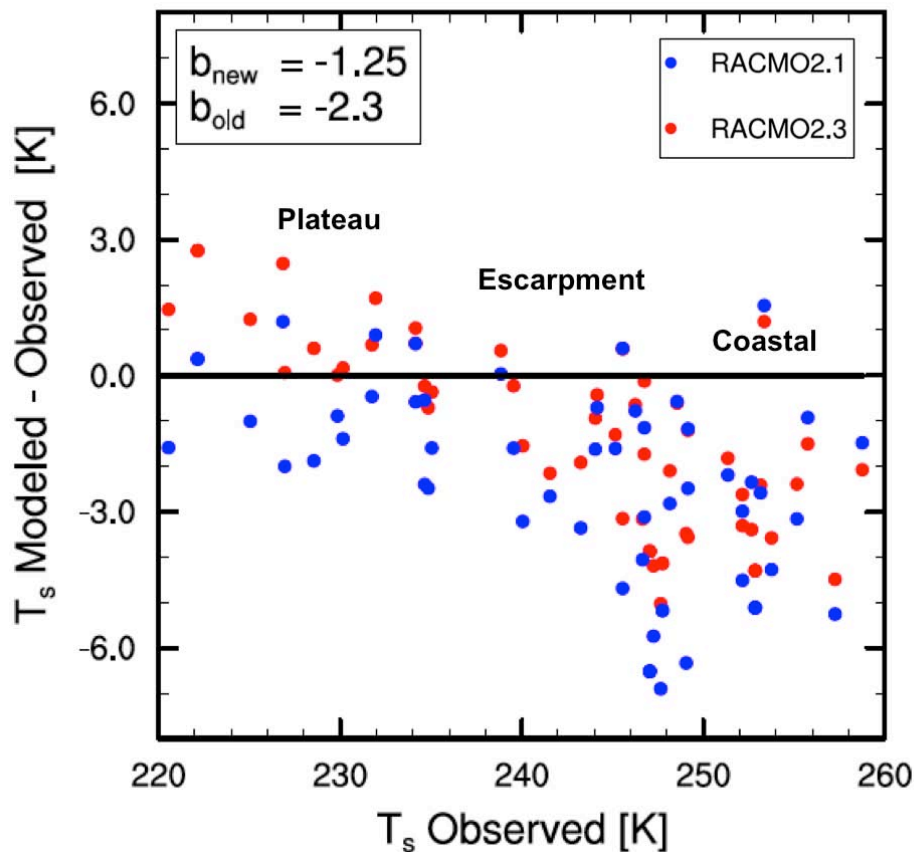
Fig. 7. Difference (modelled – observed) of the annual period averaged (1979–2011) surface temperature (T_s) as a function of 10 m ice core observations. Shown are RACMO2.3 (red) with bias b_{new} and RACMO2.1 (blue) with bias b_{old} (in [K]).

Discussion Paper | Discussion Paper | Discussion Paper | Discussion Paper

TCD

7, 3231–3260, 2013

Effects of changed cloud physics

J. M. van Wessem et al.

Title Page

Abstract   Introduction

Conclusions   References

Tables   Figures

⏮   ⏭

◀   ▶

Back   Close

Full Screen / Esc

Printer-friendly Version

Interactive Discussion

Fig. 8. Mean (1979–2011) RACMO2.3 **(a)** surface temperature (T_s [K]) and **(b)** potential temperature (Θ_s [K]) (contours) and the 10 m ice core observations (markers). For observed potential temperature surface pressure from RACMO2.3 is used.
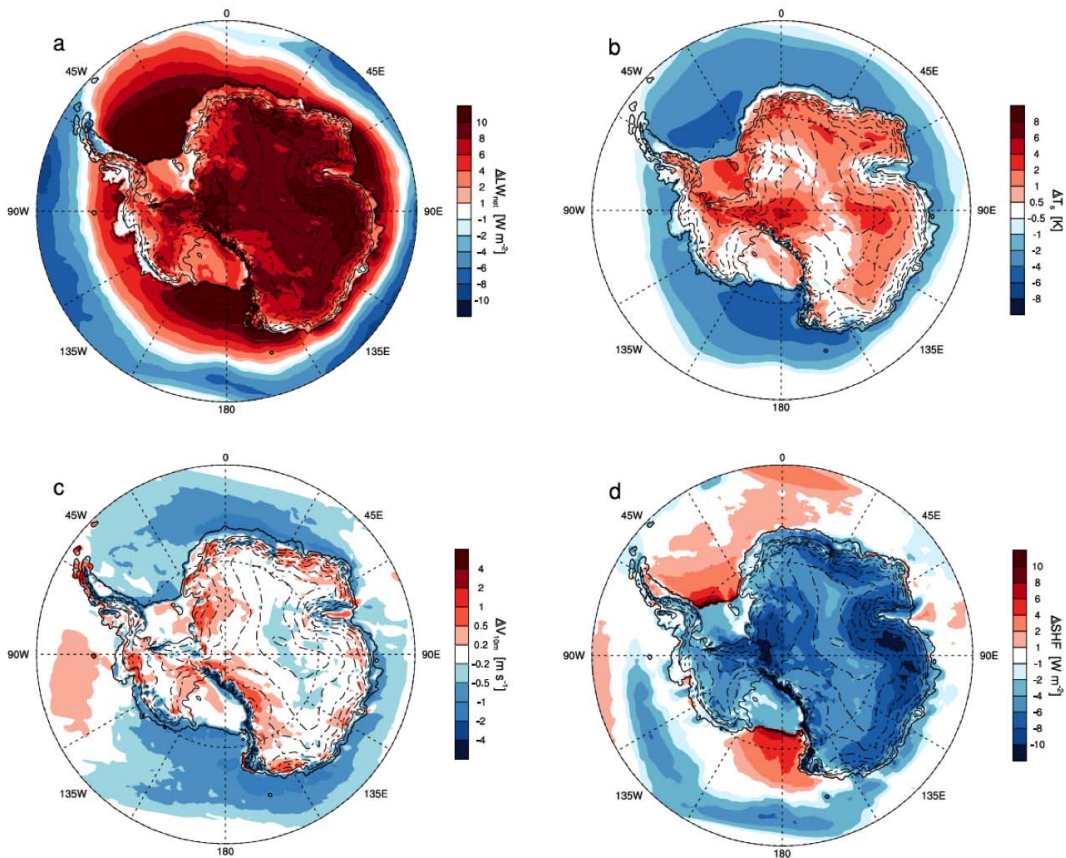
Fig. 9. Spatial distribution of difference (RACMO2.3 – RACMO2.1) for LW_{net} **(a)**, T_s **(b)**, $V_{10\,m}$ **(c)** and SHF **(d)**.

Discussion Paper

Discussion Paper

Discussion Paper

Discussion Paper

TCD

7, 3231–3260, 2013

Effects of changed cloud physics

J. M. van Wessem et al.

Title Page

Abstract | Introduction

Conclusions | References

Tables | Figures

|◄ | ►|

◄ | ►

Back | Close

Full Screen / Esc

Printer-friendly Version

Interactive Discussion
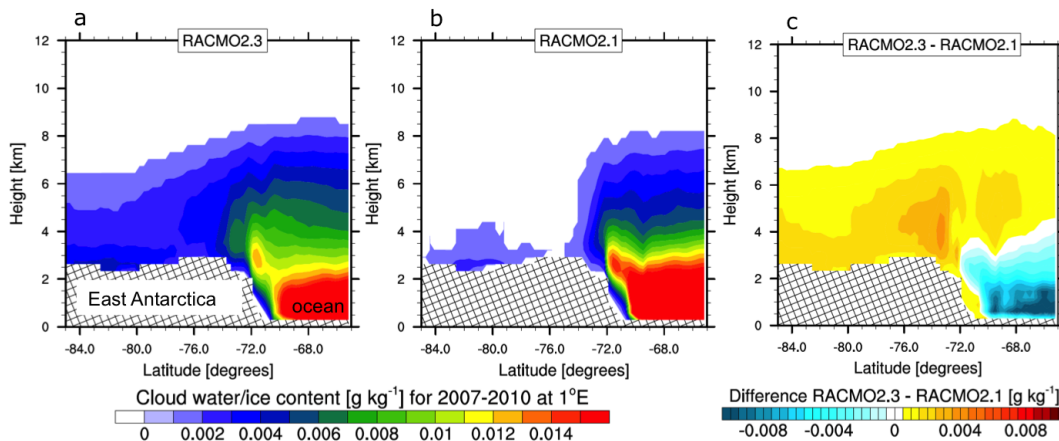
Fig. 10. Latitudinal cross-section of yearly (2007–2010) averaged total cloud water/ice content for **(a)** RACMO2.3, **(b)** RACMO2.1 and **(c)** the difference (RACMO2.3 – RACMO2.1) at 1° E. Location of cross-section is indicated in Fig. 1.
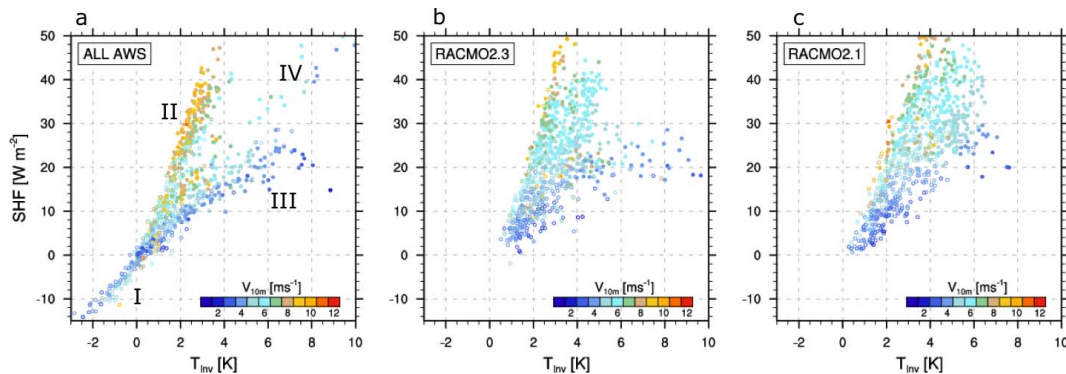
Fig. 11. Monthly averaged SHF as a function of the surface temperature inversion ($T_{inv} = T_{2\,m} - T_s$) for **(a)** all AWSs, **(b)** RACMO2.3 and **(c)** RACMO2.1. The color scheme represents wind speed $V_{10\,m}$ and model data is from the same months and locations as the observational data. Filled circles are winter values (months 4–9) and open circles represent months (10–3).